Large changes in biomass burning over the last millennium inferred from paleoatmospheric ethane in polar ice cores

Melinda R. Nicewonger[a,1], Murat Aydin[a], Michael J. Prather[a], and Eric S. Saltzman[a,b]

[a]Department of Earth System Science, University of California, Irvine, CA 92697-3100; and [b]Department of Chemistry, University of California, Irvine, CA 92697-3100

Edited by John H. Seinfeld, California Institute of Technology, Pasadena, CA, and approved October 22, 2018 (received for review May 10, 2018)

Biomass burning drives changes in greenhouse gases, climate-forcing aerosols, and global atmospheric chemistry. There is controversy about the magnitude and timing of changes in biomass burning emissions on millennial time scales from preindustrial to present and about the relative importance of climate change and human activities as the underlying cause. Biomass burning is one of two notable sources of ethane in the preindustrial atmosphere. Here, we present ice core ethane measurements from Antarctica and Greenland that contain information about changes in biomass burning emissions since 1000 CE (Common Era). The biomass burning emissions of ethane during the Medieval Period (1000–1500 CE) were higher than present day and declined sharply to a minimum during the cooler Little Ice Age (1600–1800 CE). Assuming that preindustrial atmospheric reactivity and transport were the same as in the modern atmosphere, we estimate that biomass burning emissions decreased by 30 to 45% from the Medieval Period to the Little Ice Age. The timing and magnitude of this decline in biomass burning emissions is consistent with that inferred from ice core methane stable carbon isotope ratios but inconsistent with histories based on sedimentary charcoal and ice core carbon monoxide measurements. This study demonstrates that biomass burning emissions have exceeded modern levels in the past and may be highly sensitive to changes in climate.

ethane | ice cores | biomass burning | geologic hydrocarbons | Little Ice Age

Biomass burning is a significant component of the climate system, contributing to the burden of greenhouses gases and aerosols in the atmosphere, altering the surface albedo, and affecting atmospheric chemistry. Humans have altered the natural fire landscape by introducing fires to areas that do not often burn naturally, by increasing fire ignition, and by fragmenting the natural landscape with roads, agriculture, and land management practices (1). There is controversy in the literature as to whether modern fire activity is higher or lower than in the past and the degree to which humans have altered natural fire systems (ref. 2 and references therein).

Several types of proxy records have been used to reconstruct past fire activity on centennial and millennial time scales (*SI Appendix*, Fig. S1). Ice core measurements of the abundance and stable isotopic composition of atmospheric methane (CH_4) and carbon monoxide (CO) have been used to infer global biomass burning emissions (3–6). Regional and global burning trends have also been inferred from composite charcoal records preserved in soils and lake sediments and chemical impurities (e.g., K, NH^{4+}, levoglucosan, vanillic acid) in ice cores (7–9). There is a general consensus that fire activity was high early in the past millennium [1000–1500 Common Era (CE), hereafter referred to as the Medieval Period or MP]. A decrease began during the 1400s, reaching a minimum sometime during the 1600–1800 CE cool period (Little Ice Age or LIA). However, there are inconsistencies between different records regarding the timing and magnitude of changes. For example, charcoal and CO records show that, following the LIA minimum, biomass burning emissions increased rapidly during the 1700s and 1800s and peaked during the late 19th century at rates roughly 3 to 4 times modern levels (defined as the 1997–2016 CE period of global satellite records of biomass burning). In contrast, the CH_4 stable isotope record ($\delta^{13}CH_4$) indicates that biomass burning emissions remained near their LIA minimum until about 1850 CE, when emissions began their rise to modern levels.

In this study, we use ice core measurements of ethane to reconstruct biomass burning emissions over the past millennium. Ethane (C_2H_6) is the second most abundant hydrocarbon in the atmosphere after CH_4. Ethane has an average atmospheric lifetime of roughly 2 mo due to reaction with the hydroxyl radical and a global emission rate estimated at 12 $Tg{\cdot}y^{-1}$ to 20 $Tg{\cdot}y^{-1}$ (10–16). Roughly two-thirds of global ethane emissions are related to human use of fossil fuel and biofuels (10). The remainder is derived from biomass burning and the outgassing of geologic (thermogenic) ethane from seeps (10, 11, 17). Here we show that the changes in preindustrial atmospheric ethane levels and the ethane north–south interpolar ratio over the past millennium suggest significant changes in biomass burning emissions that correlate with climate.

Ice Core Ethane Measurements

Ethane was analyzed in the air extracted from ice core samples from Greenland and Antarctica with mean gas ages ranging from 1000 CE to 1900 CE. The ice core ethane measurements reported here were conducted with an updated analytical method and constitute a significant expansion of the available data (18). The ice core site characteristics and chronologies, analytical methods

Significance

Biomass burning influences the climate system through direct emissions of aerosols, greenhouse gases, and chemically reactive gases. There is uncertainty and controversy regarding variations in past biomass burning, making it difficult to establish the climate sensitivity of biomass burning in current climate models. This study presents new measurements of ethane in air trapped in polar ice cores. The results indicate that biomass burning emissions exceeded modern levels during the Medieval Period (1000–1500 CE) but then decreased substantially during the Little Ice Age (1600–1800 CE), indicating the sensitivity of biomass burning to climate during the preindustrial era. Such positive feedbacks between biomass burning and climate may make it difficult to achieve societal climate goals.

Author contributions: M.R.N., M.A., and E.S.S. designed research; M.R.N. performed research; M.A., M.J.P., and E.S.S. contributed new reagents/analytic tools; M.R.N. and M.A. analyzed data; and M.R.N., M.A., M.J.P., and E.S.S. wrote the paper.

The authors declare no conflict of interest.

This article is a PNAS Direct Submission.

Data deposition: The ice core data reported in this paper are available at the NSF Arctic Data Center, https://arcticdata.io/ (doi.org/10.18739/A2CR5NC1B).

[1]To whom correspondence should be addressed. Email: nicewonm@uci.edu.

This article contains supporting information online at www.pnas.org/lookup/suppl/doi:10.1073/pnas.1807172115/-/DCSupplemental.

and calibration, and data quality control are discussed in *Methods* and *SI Appendix*.

The mean age of the Greenland samples (GISP2B and GISP2D ice cores) ranges from 983 CE to 1862 CE at an average resolution of 60 y (Fig. 1). Ethane in Greenland samples ranges from 446 pmol·mol^{-1} to 610 pmol·mol^{-1} with a mean of 524 ± 47 (1σ) pmol·mol^{-1}. The mean age of the Antarctic samples (WDC05A, WDC06A, and SPC14 ice cores) range from 994 CE to 1926 CE at an average resolution of 22 y (see *SI Appendix* for ice core chronologies and related uncertainties). Ethane in Antarctic samples range from 65 pmol·mol^{-1} to 167 pmol·mol^{-1} with a mean of 115 ± 22 pmol·mol^{-1}. The resulting preindustrial north–south interpolar ratio (Greenland ethane/Antarctic ethane) is roughly 4.6 ± 0.4. This ratio is reasonable given geologic ethane emissions occur mainly in the northern hemisphere. The modern (2005–2015 CE) average ethane levels over Greenland and Antarctica are roughly 1,300 and 210 pmol·mol^{-1}, respectively, resulting in a north–south interpolar ratio of about 6. Since the preindustrial period, the ice core data show a nearly threefold increase in ethane over Greenland and a twofold increase over Antarctica. These changes are in reasonable agreement with current estimates of the anthropogenic contribution to global ethane emissions (10–16).

The ice core ethane records display clear temporal variability over the past millennium. Ethane is highest during the MP, with a mean of 534 ± 26 pmol·mol^{-1} over Greenland and 130 ± 17 pmol·mol^{-1} over Antarctica, resulting in an interpolar ratio of roughly 4.2 ± 0.1 (1σ). Ethane is lowest during the LIA, when the mean ethane level is 474 ± 36 pmol·mol^{-1} over Greenland and 96 ± 15 pmol·mol^{-1} over Antarctica, resulting in an interpolar ratio of 4.9 ± 0.2. After 1850 CE, ethane levels begin to rise in both the Greenland and Antarctic records.

These variations in atmospheric ethane imply changes in either the atmospheric lifetime or emissions of ethane. The lifetime of atmospheric ethane is determined primarily by reaction with tropospheric OH (>90%), with minor losses to tropospheric Cl atoms (<5%) and stratospheric chemistry (<1%) (10). The CH_4 lifetime is a good proxy for ethane, as they have similar loss pathways and similar temperature dependence of reaction with OH.

The recent Atmospheric Chemistry and Climate Model Intercomparison Project intercomparison of chemistry/climate models showed a multimodel mean change in CH_4 lifetime from preindustrial (1850 CE) to modern (2000 CE) of $\tau_{modern}/\tau_{1850} = 2.0 \pm 8.8\%$ (19). The models were split between positive and negative changes in CH_4 lifetime. In other words, current chemistry/climate models disagree on the magnitude and sign of the change, but there is strong consensus that the change in CH_4 lifetime from the preindustrial to modern was less than ±10%. This change is influenced by several competing factors: (*i*) increased CH_4, which has the net effect of suppressing OH; (*ii*) increased CO and NOx, which increase tropospheric ozone, the primary source of OH; (*iii*) loss of stratospheric ozone resulting in increased UV radiation; and (*iv*) increased global temperature, which increases water vapor (and OH production) but also increases rate constants, including that for reaction of OH with ethane. Naik et al. (19) suggest that, of these four factors, the differences in CO and NOx variability/chemistry appear to contribute most to the OH variance between model simulations from preindustrial to modern.

The ice core ethane records presented here cover 1000–1900 CE. Atmospheric impacts of industrialization start to become apparent after 1850 CE, with the bulk of the changes occurring during the 20th century. Before 1850 CE, atmospheric CH_4 was relatively stable in the 650 nmol·mol^{-1} to 800 nmol·mol^{-1} range, and global temperature variations were about 0.5 °C, less than half of the >1 °C rise that followed (20). Preindustrial changes in NOx were likely also small, based on the <20% variability in Greenland ice core nitrate before 1850 CE, compared with the near doubling since 1850 CE (21). Ice core data suggest that preindustrial CO variability was comparable to or less than the CO change during industrialization (6, 22). Based on the ice core CO stable isotope measurements, Wang et al. (6) suggest that most of the preindustrial CO variability was driven by changes in emissions rather than OH. There is no evidence to suggest that OH variability in the preindustrial atmosphere was larger than the 10% upper limit suggested for the preindustrial to modern change. Therefore, we assume that ice core ethane variability is primarily driven by changes in emissions rather than atmospheric reactivity.

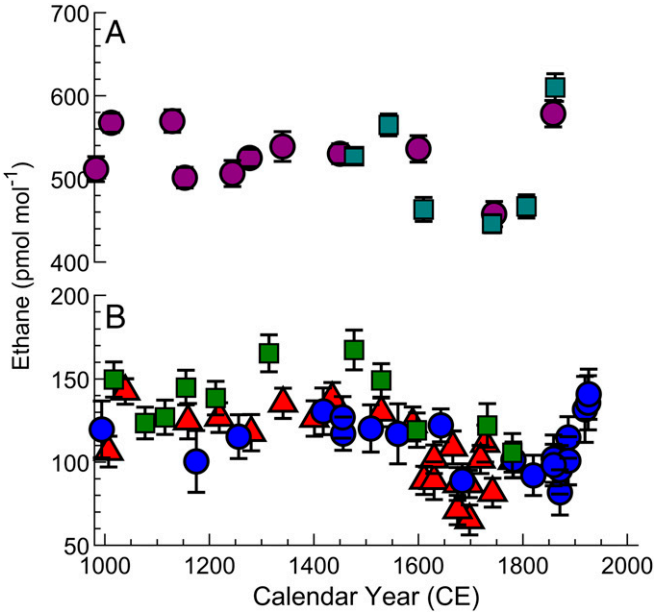

Fig. 1. (*A*) Greenland ice core ethane levels from GISP2B (teal squares) and GISP2D (purple circles). (*B*) Antarctic ice core ethane levels from SPC14 (green squares), WDC06A (red triangles), and WDC05A (blue circles). Error bars are 1σ uncertainty.

Models Calculations to Infer the Causes of Variations in Paleoatmospheric Ethane

Ethane is considerably shorter-lived in the atmosphere than CH_4 (2 mo to 3 mo vs. 9 y to 12 y). The ethane atmospheric mixing ratio exhibits significant regional, hemispheric, and seasonal variability, reflecting the distribution of various sources and the effects of atmospheric reactivity and transport. These complexities must be taken into account to infer the changes in emissions that can drive the variations apparent in the ice core ethane records. We used a 3D chemical transport model [University of California, Irvine 3D Chemical Transport Model (UCI-CTM); see *Methods*] to estimate the sensitivity of ethane levels over Antarctica and Greenland to various ethane sources (23, 24). This was done by defining a reference model simulation of the modern atmosphere and adding an ethane-like tracer species. This tracer reacts in the model with the same OH lifetime and stratospheric loss rate as ethane but does not affect the reference chemistry. This approach is suitable because ethane, unlike CH_4 or CO, does not significantly impact tropospheric photochemistry (25). Sensitivity runs were carried out whereby particular source regions of the ethane-like tracer were given a fixed emission (teragrams per year), and the steady-state sensitivity was calculated for both Greenland and Antarctica as follows: pmol·mol$^{-1}{}_{\text{ethane tracer}}$/Tg·y$^{-1}{}_{\text{ethane tracer}}$.

Sensitivities were computed for the atmosphere over Antarctica and Greenland for biomass burning, biofuel, and geologic emissions. *SI Appendix*, Table S1 shows the spatial/temporal distributions specified for each source and the resulting model sensitivities for Antarctica and Greenland. We assume that the geographic distribution of these sources does not change over time. As expected, Antarctic ethane levels are more sensitive to biomass burning emissions from nonboreal regions which are located primarily in the tropics than to biofuel or geological emissions which are located primarily in the Northern Hemisphere midlatitudes. Additionally, Greenland ethane levels are highly sensitive to boreal burning which occurs in close proximity to that region.

Using the model sensitivities, the ethane levels over Antarctica and Greenland can be calculated for a given emissions scenario by summing over the various types of emissions each multiplied by the sensitivity of that emission type. The ice core data were divided into two periods: (*i*) MP and (*ii*) LIA. A Boolean cost function (CF) was used to determine the viable emission scenarios during these two periods by comparing the modeled ethane levels over Greenland and Antarctica to the mean ice core ethane data for the MP and LIA as follows:

$$\mathrm{CF}_{\mathrm{ethane}} = \frac{|m_{\mathrm{grn}} - o_{\mathrm{grn}}|}{o_{\mathrm{grn}}} < 0.1 \text{ and } \frac{|m_{\mathrm{ant}} - o_{\mathrm{ant}}|}{o_{\mathrm{ant}}} < 0.1, \quad [1]$$

where m stands for the modeled value and o stands for the observed mean level from the ice core record from Greenland (grn) and Antarctica (ant). For a scenario to be considered valid, both the Greenland and Antarctic ethane levels must be within 10% of the observed mean ice core ethane level for the MP and LIA periods.

Ethane shares similar sources with atmospheric CH_4 through geologic outgassing and biomass burning. A steady-state atmospheric box model was used to calculate the atmospheric CH_4 mixing ratio and $\delta^{13}CH_4$ for various emission scenarios. This allowed us to assess how the inferred biomass burning history compares to the ice core CH_4 and $\delta^{13}CH_4$ (see *Methods*). The modeled CH_4 levels were compared with previous ice core measurements of CH_4 and $\delta^{13}CH_4$ (4, 26, 27), and a CF value was calculated as follows:

$$\mathrm{CF}_{\mathrm{CH_4}} = \frac{|m_{[\mathrm{CH_4}]} - o_{[\mathrm{CH_4}]}|}{o_{[\mathrm{CH_4}]}} < 0.1 \text{ and } \frac{|m_{\delta^{13}\mathrm{CH_4}} - o_{\delta^{13}\mathrm{CH_4}}|}{|\delta^{13}\mathrm{CH_4\_max} - \delta^{13}\mathrm{CH_4\_min}|} < 0.1. \quad [2]$$

The denominator in the second part of the calculation is the absolute value of the observed range in the $\delta^{13}CH_4$ ice core record over the 1,000-y period, roughly 3‰.

Modeling Results

Ethane. There are three major ethane sources to the preindustrial atmosphere: biomass burning, biofuel, and geologic emissions. The ice core data from Antarctica and Greenland provide only two mass balance constraints. As an additional constraint, we prescribe a constant 0.5 $Tg{\cdot}y^{-1}$ of emissions from biofuel burning, adopting the estimate of van Aardenne et al. (28). We then conduct a grid search by varying biomass burning from 0 $Tg{\cdot}y^{-1}$ to 5 $Tg{\cdot}y^{-1}$ and geologic emissions from 0 $Tg{\cdot}y^{-1}$ to 6 $Tg{\cdot}y^{-1}$ independently for the MP and the LIA and calculate the CF to find solutions that explain the ice core data. Spatial patterns and seasonality of biomass burning emissions are assumed to be identical to today as represented by Global Fire Emissions Database version 3 (GFED3) (29). Agreement within 10% of the ice core data requires geologic ethane emissions of ~6 $Tg{\cdot}y^{-1}$ for the MP and slightly less, near ~5 $Tg{\cdot}y^{-1}$, for the LIA (Fig. 2*A* and *SI Appendix*, Fig. S2). These estimates are higher than the bottom-up estimates of geologic ethane emissions, which range from 2 $Tg{\cdot}y^{-1}$ to 4 $Tg{\cdot}y^{-1}$ (17). Strong geologic ethane sources are required to reproduce the large north–south interpolar ratio between Greenland and Antarctic ice core records, since most geologic emissions occur in the Northern Hemisphere. The range of emissions identified as viable in this analysis requires slightly lower geologic emissions during the LIA than the MP. It is not clear why geologic emissions would vary during the preindustrial period. Processes that can impact geologic emissions (e.g., plate tectonic motions and sea level change) vary on longer time scales. The viable solutions found in this analysis require a strong and variable geologic ethane source, and this does not appear to be realistic. As an alternative, we explore the possibility that the spatial footprint of ethane sources in the preindustrial atmosphere was not the same as in the modern atmosphere.

To provide flexibility in the distribution of emissions, we allowed boreal (defined here as >50°N) and nonboreal (50°N to 90°S) biomass burning emissions to vary independently. Based on the GFED3 inventory, roughly 10% of global biomass burning ethane emissions are in the boreal region, and nearly 88% of emissions are in the tropics (30°N to 30°S). The remainder (<3%) occurs outside the tropics in the temperate regions (ref. 29 and *SI Appendix*, Fig. S3). Although boreal burning emissions are relatively small compared with nonboreal emissions, they exert a disproportionately strong influence on ethane levels over Greenland (*SI Appendix*, Table S1). By contrast, the sensitivities of Greenland and Antarctic ethane levels to nonboreal (mostly tropical) burning emissions are similar.

We conducted another grid search, allowing boreal burning emissions to range from 0 $Tg{\cdot}y^{-1}$ to 3 $Tg{\cdot}y^{-1}$, nonboreal emissions to range from 0 $Tg{\cdot}y^{-1}$ to 5 $Tg{\cdot}y^{-1}$, and geologic emissions to range from 0 $Tg{\cdot}y^{-1}$ to 6 $Tg{\cdot}y^{-1}$. It was possible to find solutions which successfully reconstruct the Greenland and Antarctic ice core data for both the MP and LIA while maintaining temporally constant geologic emissions within the 2 $Tg{\cdot}y^{-1}$ to 4 $Tg{\cdot}y^{-1}$ range estimated by Etiope and Ciccioli (17) (Fig. 2*B* and *SI*

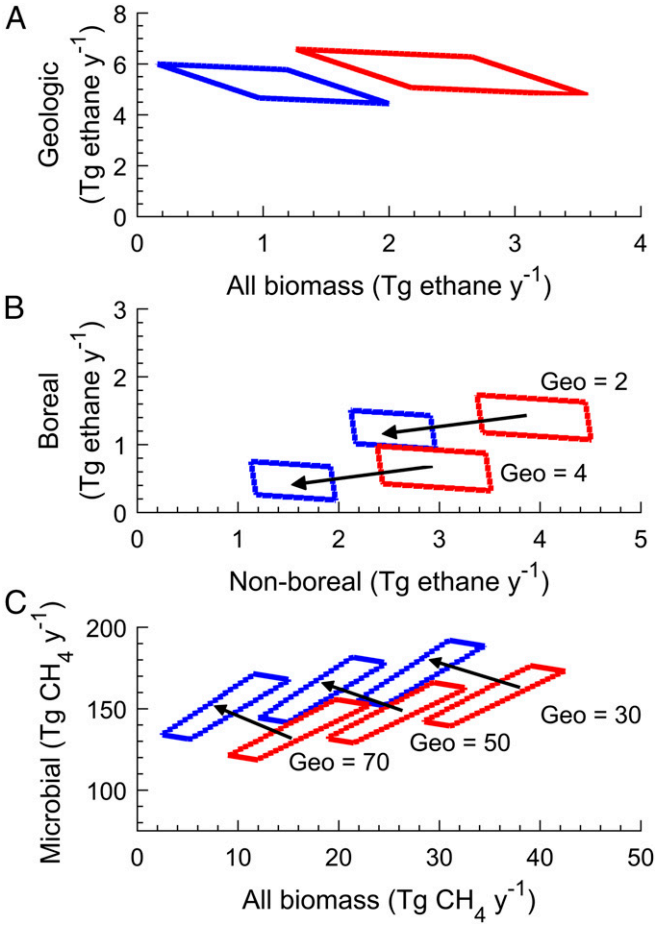

Fig. 2. Model results for ethane and CH_4 showing the range of emissions that are consistent with the ice core data given various assumptions about geologic emissions. The lines enclose regions with successful emission scenarios, and the arrows connect the MP (red) to LIA (blue) results for specified geologic emissions. (*A*) Ethane scenarios with varying biomass burning and geologic emissions. (*B*) Ethane scenarios allowing boreal and nonboreal emissions to vary independently, with fixed geologic emissions. (*C*) CH_4 scenarios allowing microbial and biomass burning emissions to vary, with fixed geologic emissions.

Appendix, Fig. S4 and Table S2). For example, at geologic ethane emissions of 2 $Tg{\cdot}y^{-1}$, agreement with the MP ice core data is obtained for nonboreal burning emissions in the range of 3.7 $Tg{\cdot}y^{-1}$ to 4.3 $Tg{\cdot}y^{-1}$ and boreal emissions in the range of 1.2 $Tg{\cdot}y^{-1}$ to 1.6 $Tg{\cdot}y^{-1}$. During the LIA for the same geologic emissions, the estimates of nonboreal and boreal emissions decrease to 2.3 $Tg{\cdot}y^{-1}$ to 2.7 $Tg{\cdot}y^{-1}$ and 1.1 $Tg{\cdot}y^{-1}$ to 1.3 $Tg{\cdot}y^{-1}$, respectively. By design, higher geologic emissions require less biomass burning emissions to fit the ethane ice core records during both the MP and LIA, but the magnitude of fire emission decrease from the MP to LIA does not change significantly (Fig. 2*B*).

There are some robust conclusions that can be drawn from these results. The total (boreal and nonboreal) decline in biomass burning ethane emissions from the MP to the LIA is roughly 1.5 $Tg{\cdot}y^{-1}$, which is 30 to 45% of the burning emissions during the MP, depending on whether the geologic emissions are at the lower or higher end of the 2 $Tg{\cdot}y^{-1}$ to 4 $Tg{\cdot}y^{-1}$ range (Fig. 3*A*). Most of the decrease in biomass burning emissions results from a reduction in nonboreal fires. Boreal emissions decreased between 13% and 27%, while nonboreal emissions decreased by 35 to 47% (Fig. 2*B*). We estimate total biomass burning ethane emissions during the MP to be 3.7 $Tg{\cdot}y^{-1}$ to 5.4 $Tg{\cdot}y^{-1}$ (*SI Appendix*, Table S2), which is higher than estimates of modern biomass burning ethane emissions based on satellite measurements of global dry matter burned and emission factors (3.4 ± 0.2 $Tg{\cdot}y^{-1}$, mean ±1 SE; ref. 30). During the LIA, total burning emissions range from 2.1 $Tg{\cdot}y^{-1}$ to 3.7 $Tg{\cdot}y^{-1}$, which is the same as biomass burning emissions today. Both boreal and nonboreal burning ethane emissions decrease from the MCA to LIA, but the magnitude of the decrease is larger in nonboreal ethane emissions.

The boreal component in our emission estimates ranges from 0.7 $Tg{\cdot}y^{-1}$ to 1.4 $Tg{\cdot}y^{-1}$ during the MP and 0.5 $Tg{\cdot}y^{-1}$ to 1.2 $Tg{\cdot}y^{-1}$ during the LIA. Modern mean boreal ethane emissions are estimated to be 0.6 ± 0.2 $Tg{\cdot}y^{-1}$ (mean ± 1 SE; ref. 30). Most of the viable solutions require a stronger preindustrial boreal component than what is in the GFED4 emissions inventory (30). Higher preindustrial boreal ethane emissions do not necessarily require higher burning rates (in terms of kilograms dry matter burned per year) but could instead be related to emission factors and the uncertainties in these factors used to calculate boreal ethane emissions (31). The requirement of higher boreal ethane emissions could also indicate that the chemical transport model used in this study underestimates the efficiency of transport of boreal fire emissions to the Arctic (and hence the sensitivity in our model calculations). Simulating the chemical transport between midlatitudes and the Arctic occurs on spatial and temporal scales that present challenges to global transport models (32).

Methane. An important test for the validity of these inferences from the ethane data is to determine whether the successful emissions scenarios are consistent with ice core CH_4 and $\delta^{13}CH_4$ records (4, 26, 27). During the MP, atmospheric CH_4 levels are around 680 $nmol{\cdot}mol^{-1}$ and $\delta^{13}CH_4$ is rather heavy, near –47.4‰. Heading into the LIA, CH_4 levels are rising, while $\delta^{13}CH_4$ decreases to around –48.9‰. Using the atmospheric CH_4 box model and CF described earlier, we determined viable emission scenarios for CH_4 during the MP and LIA. Geologic, microbial (wetlands and agriculture), and biomass burning CH_4 emissions were allowed to range from 0 $Tg{\cdot}y^{-1}$ to 70 $Tg{\cdot}y^{-1}$, 50 $Tg{\cdot}y^{-1}$ to 200 $Tg{\cdot}y^{-1}$, and 0 $Tg{\cdot}y^{-1}$ to 50 $Tg{\cdot}y^{-1}$, respectively. Emission scenarios which satisfy the CH_4 CF are shown in Fig. 2*C*. See *SI Appendix*, Fig. S5 and Table S3 for the full solution space. We maintained the requirement that geologic CH_4 emissions did not change from the MP to the LIA. All viable solutions require some shifting from isotopically heavy CH_4 sources (geologic or biomass burning) to isotopically lighter sources (wetlands, agriculture) to satisfy the higher levels of CH_4 that is isotopically lighter during the LIA (*SI Appendix*, Table S3). For example, with geologic CH_4 emissions at 50 $Tg{\cdot}y^{-1}$, agreement with the MP ice core data occurs with microbial emissions in the range of 138 $Tg{\cdot}y^{-1}$ to 158 $Tg{\cdot}y^{-1}$ and biomass burning emissions of 23 $Tg{\cdot}y^{-1}$ to 29 $Tg{\cdot}y^{-1}$. For the LIA and same geologic emissions, microbial emissions increase to 151 $Tg{\cdot}y^{-1}$ to 174 $Tg{\cdot}y^{-1}$, and biomass burning emissions decrease to 16 $Tg{\cdot}y^{-1}$ to 22 $Tg{\cdot}y^{-1}$.

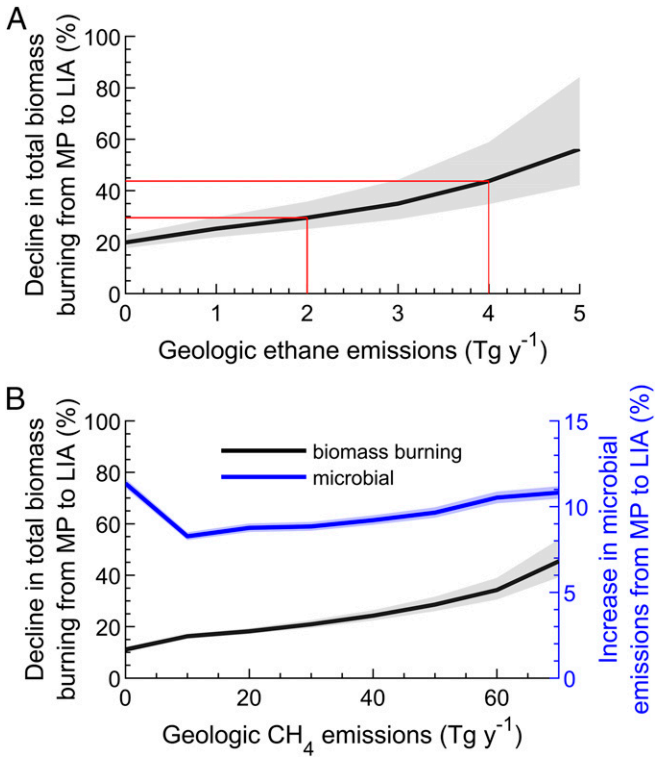

Fig. 3. Modeled percent change in ethane and CH_4 emissions between the MP and LIA calculated as 100*(MP – LIA)/MP. Shaded areas represent the 1σ uncertainty. (*A*) Change in total biomass burning ethane emissions for a range of geologic emissions (red lines denote best estimate of 2 $Tg{\cdot}y^{-1}$ to 4 $Tg{\cdot}y^{-1}$). (*B*) Change in total biomass burning (black) and microbial (blue) CH_4 emissions for geologic CH_4 emissions ranging from 0 $Tg{\cdot}y^{-1}$ to 70 $Tg{\cdot}y^{-1}$.

The successful CH_4 scenarios indicate that biomass burning CH_4 emissions deceased by about 7 $Tg{\cdot}y^{-1}$ from the MP to the LIA, regardless of the geologic emissions specified. Because of the long atmospheric lifetime of CH_4 (compared with ethane), we do not distinguish between boreal and nonboreal biomass burning emissions of CH_4. The ethane analysis showed that the percent decline in total biomass burning from the MP to LIA was 30 to 45% and largely driven by nonboreal emissions. The 7 $Tg{\cdot}y^{-1}$ decline in CH_4 emissions from biomass burning should also correspond to roughly the same percent decline. This occurs when geologic CH_4 emissions range from 50 $Tg{\cdot}y^{-1}$ to 70 $Tg{\cdot}y^{-1}$ (Fig. 3*B*), which agrees with top-down and bottom-up estimates of geologic CH_4 emissions (18, 33, 34). The viable scenarios all require that microbial emissions increase by roughly 15 $Tg{\cdot}y^{-1}$ or about 10% from the MP to the LIA (Fig. 3*B*). These findings are entirely consistent with previous modeling studies of ice core CH_4 and $\delta^{13}CH_4$ from this period (3–5).

The scenarios identified as viable for both ethane and CH_4 are mutually consistent, based on our understanding of the CH_4/ethane ratios of major sources today. We illustrate this in Fig. 4 using geologic ethane and CH_4 emissions of 3 $Tg{\cdot}y^{-1}$ and 60 $Tg{\cdot}y^{-1}$, which lie in the middle of their estimated ranges. During the MP, ethane and CH_4 burning emissions are 4.4 and 21.0 $Tg{\cdot}y^{-1}$, respectively, which implies a CH_4/ethane emission ratio of 4.8 (teragrams per teragram). During the LIA, total burning ethane and CH_4 emissions decrease to 2.8 and 13.7 $Tg{\cdot}y^{-1}$, respectively, implying a CH_4/ethane emission ratio from biomass burning of 4.9. The average CH_4 to ethane emission ratio from modern biomass burning is estimated to be 5.1 ± 2.4 (31). This analysis shows that the decline in ice core ethane and $\delta^{13}CH_4$ from MP to

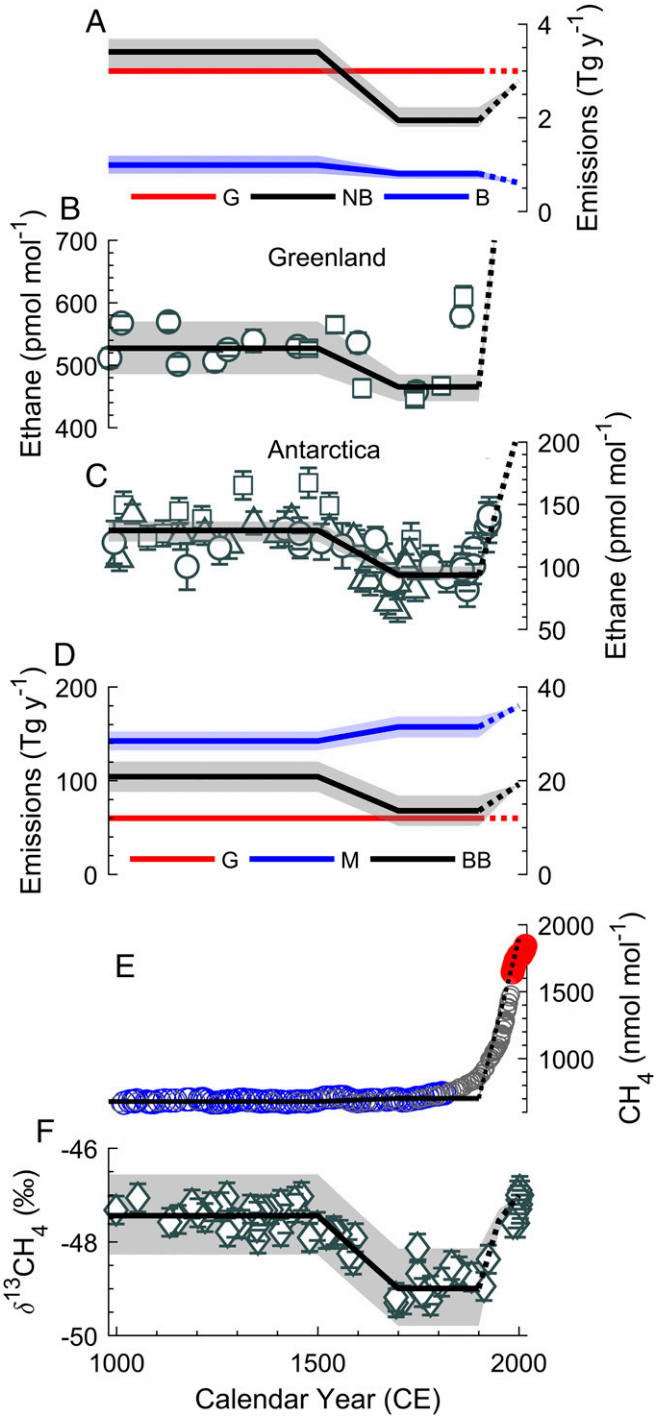

Fig. 4. Valid ethane and CH_4 emission scenarios for the last millennium with geologic emissions fixed in the middle of the range of best estimates (3 Tg·y^{-1} for ethane and 60 Tg·y^{-1} for CH_4). In all panels, the solid line and shaded areas represent the mean and range, respectively, and the dashed line after 1900 CE is a linear interpolation between the modeled LIA budget and the modern budget (*SI Appendix*, Table S6). (*A*) Ethane budget with geologic (G, red), boreal (B, blue), and nonboreal (NB, black) emissions. During the MP, boreal and nonboreal ethane emissions range from 0.8 Tg·y^{-1} to 1.2 Tg·y^{-1} and 3.1 Tg·y^{-1} to 3.7 Tg·y^{-1}, respectively. During the LIA, boreal and nonboreal ethane emissions range from 0.7 Tg·y^{-1} to 0.9 Tg·y^{-1} and 1.8 Tg·y^{-1} to 2.2 Tg·y^{-1}, respectively. (*B*) Greenland ethane levels resulting from the budget in *A*. (*C*) Antarctic ethane levels resulting from the budget in *A*. (*D*) CH_4 budget with geologic (G; red, left axis), microbial (M; blue, left axis), and biomass burning (BB; black, right axis) emissions. During the MP, microbial and biomass burning emissions range from 133 Tg·y^{-1} to 153 Tg·y^{-1} and 18 Tg·y^{-1} to 24 Tg·y^{-1}, respectively. During the LIA, microbial and biomass burning emissions range from 146 Tg·y^{-1} to 169 Tg·y^{-1} and 11 Tg·y^{-1} to 17 Tg·y^{-1}. (*E*) Atmospheric CH_4 levels resulting from the budget in *D*. Atmospheric CH_4 measurements (circles) from refs. 26, 27, and 35. (*F*) Atmospheric $\delta^{13}CH_4$ resulting from the budget in *D*. Atmospheric $\delta^{13}CH_4$ measurements (diamonds) are from ref. 4.

LIA can be attributed to a large percent decrease in global biomass burning without requiring significant temporal changes in CH_4/ethane emission ratios associated with burning.

Conclusions

The analysis and interpretation of ice core ethane in Greenland and Antarctic ice cores provides constraints on past changes in global biomass burning emissions. The ethane atmospheric histories and interpolar difference are consistent with the observed changes in ice core CH_4 and $\delta^{13}CH_4$. The ethane data impose an additional constraint that either (*i*) boreal biomass burning is a slightly larger fraction of total burning emissions than currently estimated (based on satellite data and emission ratios) or (*ii*) boreal fire emissions are more efficiently transported to the Arctic atmosphere in reality than in our chemical transport model. Because boreal emissions are a relatively small component of the overall global biomass burning emissions, both are viable possibilities within the uncertainties in the current budget.

The new ice core ethane data and the existing CH_4 and $\delta^{13}CH_4$ records (3–5) support a 30 to 45% decrease in biomass burning emissions from 1500 CE to 1700 CE. This is considerably smaller than the fourfold change in emissions inferred from the CO record (6). The ethane and CH_4 records indicate that the relatively low burning emissions of the LIA persisted until the onset of fossil fuel hydrocarbon emissions in the mid-to-late 1800s. In contrast to the ice core CO or sedimentary charcoal records, there is no evidence in the ice core ethane records to support a steep rise in biomass burning around 1750 CE (6, 7). The ethane record indicates that biomass burning ethane emissions during the MP were greater than modern rates.

There are several reasons why biomass burning records based on ice core trace gases might differ from those based on sedimentary charcoal. First, sedimentary charcoal records are qualitative and require normalization to develop regional averages. Second, they provide limited information about fires in low-wood biomes, such as savannas and grasslands, which comprise over 40% of pyrogenic carbon emissions globally (29). By contrast, biomass burning histories based on ice core ethane, $\delta^{13}CH_4$, and CO (and its stable isotopes) measurements should all agree within the uncertainties. The discrepancies apparent between the CO and hydrocarbon-based records highlight the need for comeasurements of all biomass burning-related trace gases in multiple ice cores. In particular, it is necessary to replicate the ethane record from Greenland ice cores at a higher resolution to better characterize the biomass burning low during the LIA.

The decrease in ethane emissions during the cool LIA supports the idea that biomass burning is sensitive to climate. This decrease was driven mainly by a decline in emissions from the nonboreal region, which is mostly comprised of tropical emissions. This provides additional evidence that the LIA influenced climate conditions globally and was not simply a regional phenomenon restricted to the extratropical Northern Hemisphere (36).

There has been debate about whether biomass burning rates increased during industrialization due to deforestation and agriculture or decreased because of fire suppression (ref. 37 and references within). Our analysis shows that LIA biomass burning ethane emissions ranged from 2.1 Tg·y^{-1} to 3.7 Tg·y^{-1}. The satellite-based estimate of modern biomass burning ethane emissions is 3.4 ± 0.2 Tg·y^{-1}, which falls within the LIA range (30). Within the uncertainties of the ice core ethane analysis, we cannot determine whether anthropogenic activities had a significant impact on global biomass burning emissions since the LIA.

A full understanding of the processes controlling changes in biomass burning emissions over the past millennium requires both a longer atmospheric history covering a wider range of climate variability and knowledge of the spatial patterns of these changes. Thus, the challenge remains to reconcile these results with the CO record and more spatially resolved proxies (such as sedimentary charcoal, tree fire scars, aerosol-borne ice core chemicals, and ice core black carbon).

Methods

Analytical Methods. Air bubbles were extracted from 300- to 380-g ice core samples by melting under vacuum (18). The wet-extraction system consists of an all-glass vacuum line with flat glass flanges sealed with indium O-rings (Indium Wire Extrusion) and Teflon-sealed glass valves (Glass Expansion Australia). Samples are mechanically cleaned and placed in a glass chamber precooled to −40 °C. The chamber is repeatedly flushed with N_2 and isolated from the vacuum line, and the sample is melted. The evolved air is cryogenically pumped into a stainless steel tube (at 4 K) and isolated with a bellows valve (Swagelok Co). Ethane is analyzed by gas chromatography with high-resolution mass spectrometry. An internal standard containing $^{13}C_2H_6$ is added to the sample (18, 38). Calibration is based on high-pressure standards prepared in our laboratory. Analytical blanks are estimated by adding N_2 over the refrozen sample, melting the sample, extracting, and analyzing as above. The ethane abundance in each sample is corrected by subtracting the mean blank from a succession of samples (*SI Appendix*).

Chemical Transport Model. UCI-CTM was used to estimate the sensitivity of ethane levels over Greenland and Antarctica to various ethane sources. UCI-CTM was used with a resolution of ~2.8° × 2.8°, 57 vertical layers, and European Centre for Medium-Range Weather Forecasts meteorological fields (2005–2007) (23, 24). Annual average air mass-weighted mixing ratios from the final year of the simulations were used. Fossil fuel ethane emissions were based on the representative concentration pathway (RCP) year 2000 inventory (39), and biomass burning ethane emissions were based on GFED3.1 (29). OH oxidation kinetics from ref. 40 were used.

Methane Box Model. The steady-state atmospheric box model includes emissions from biogenic (wetlands, agriculture), biomass and biofuel burning, and geologic outgassing. The $^{13}C/^{12}C$ ratios were assigned to each source (41), and rate constants for each CH_4 loss pathway (OH, soil, stratosphere) were based on published estimates and isotopic fractionation factors (*SI Appendix* and ref. 4). The atmospheric lifetime of CH_4 in the model is set to 9.5 y, based on the 3D global OH and temperature distributions (42) and temperature-dependent reaction rate constant (43). The model solves the mass balance equations for CH_4, $^{12}CH_4$, and $^{13}CH_4$. The results are reported as CH_4 mixing ratio and $\delta^{13}CH_4$ (*SI Appendix*).

ACKNOWLEDGMENTS. We thank National Science Foundation (NSF) Ice Core Facility for assistance in obtaining ice core samples and Xin Zhu for assistance with UCI-CTM. This research was supported by NSF Grant OPP-1644245, NSF Graduate Research Fellowship Program Award DGE-1321846 (to M.R.N.), NASA Grant NNX15AE35G, and the NSF Independent Research/Development program (E.S.S.).

1. Bowman DMJS, et al. (2011) The human dimension of fire regimes on Earth. *J Biogeogr* 38:2223–2236.
2. van der Werf GR, Peters W, van Leeuwen TT, Giglio L (2013) What could have caused pre-industrial biomass burning emissions to exceed current rates? *Quat Sci Rev* 9: 289–306.
3. Ferretti DF, et al. (2005) Unexpected changes to the global methane budget over the past 2000 years. *Science* 309:1714–1717.
4. Mischler JA, et al. (2009) Carbon and hydrogen isotopic composition of methane over the last 1000 years. *Global Biogeochem Cycles* 23:GB4024.
5. Sapart CJ, et al. (2012) Natural and anthropogenic variations in methane sources during the past two millennia. *Nature* 490:85–88.
6. Wang Z, Chappellaz J, Park K, Mak JE (2010) Large variations in Southern Hemisphere biomass burning during the last 650 years. *Science* 330:1663–1666.
7. Marlon JR, et al. (2008) Climate and human influences on global biomass burning over the past two millennia. *Nat Geosci* 2:697–702.
8. Grieman MM, Aydin M, Isaksson E, Schwikowski M, Saltzman ES (2018) Aromatic acids in an Arctic ice core from Svalbard: A proxy record of biomass burning. *Clim Past* 14: 637–651.
9. Legrand M, et al. (2016) Boreal fire records in Northern Hemisphere ice cores: A review. *Clim Past* 12:2033–2059.
10. Xiao Y, et al. (2008) Global budget of ethane and regional constraints on U.S. sources. *Quat Sci Rev* 113:D21306.
11. Simpson IJ, et al. (2012) Long-term decline of global atmospheric ethane concentrations and implications for methane. *Nature* 488:490–494.
12. Aydin M, et al. (2011) Recent decreases in fossil-fuel emissions of ethane and methane derived from firn air. *Nature* 476:198–201.
13. Dalsøren SB, et al. (2018) Discrepancy between simulated and observed ethane and propane levels explained by underestimated fossil emissions. *Nat Geosci* 11:178–184.
14. Franco B, et al. (2016) Evaluating ethane and methane emissions associated with the development of oil and natural gas extraction in North America. *Environ Res Lett* 11: 044010.
15. Helmig D, et al. (2016) Reversal of global atmospheric ethane and propane trends largely due to US oil and natural gas production. *Nat Geosci* 9:490–495.
16. Tzompa-Sosa ZA, et al. (2017) Revisiting global fossil fuel and biofuel emissions of ethane. *J Geophys Res* 122:2493–2512.
17. Etiope G, Ciccioli P (2009) Earth's degassing: A missing ethane and propane source. *Science* 323:478.
18. Nicewonger MR, Verhulst KR, Aydin M, Saltzman ES (2016) Preindustrial atmospheric ethane levels inferred from polar ice cores: A constraint on the geologic sources of atmospheric ethane and methane. *Geophys Res Lett* 43:1–8.
19. Naik V, et al. (2013) Preindustrial to present-day changes in tropospheric hydroxyl radical and methane lifetime from the Atmospheric Chemistry and Climate Model Intercomparison Project (ACCMIP). *Atmos Chem Phys* 13:5277–5298.
20. PAGES 2K Consortium (2013) Continental-scale temperature variability during the past two millennia. *Nat Geosci* 6:339–346.
21. Fischer H, Wagenbach D, Kipfstuhl J (1998) Sulfate and nitrate firn concentrations on the Greenland ice sheet: 2. Temporal anthropogenic deposition changes. *J Geophys Res* 103:21935–21942.
22. Hann D, Raynaud D (1998) Ice core record of CO variations during the last two millennia: Atmospheric implications and chemical interactions within the Greenland ice. *Tellus B Chem Phys Meterol* 50:253–262.
23. Prather MJ, Hsu J (2010) Coupling of nitrous oxide and methane by global atmospheric chemistry. *Science* 330:952–954.
24. Holmes CD, Prather MJ, Søvde AO, Myhre G (2013) Future methane, hydroxyl, and their uncertainties: Key climate and emission parameters for future predictions. *Atmos Chem Phys* 13:285–302.
25. Prather MJ (1994) Lifetimes and eigenstates in atmospheric chemistry. *Geophys Res Lett* 21:801–804.
26. Mitchell LE, Brook EJ, Sowers T, McConnell JR, Taylor K (2011) Multidecadal variability of atmospheric methane, 1000–1800 C.E. *J Geophys Res Biogeosci,* 116:G02007.
27. Etheridge DM, Steele LP, Francey RJ, Langenfelds RL (1998) Atmospheric methane between 1000 A.D. and present: Evidence of anthropogenic emissions and climatic variability. *J Geophys Res* 103:15979–15993.
28. van Aardenne JA, Dentener FJ, Olivier JGJ, Goldewijk CGMK, Lelieveld J (2001) A 1x1 resolution data set of historical anthropogenic trace gas emissions for the period 1890–1990. *Global Biogeochem Cycles* 15:909–928.
29. van der Werf GR, et al. (2010) Global fire emissions and the contribution of deforestation, savanna, forest, agricultural, and peat fires (1997-2009). *Atmos Chem Phys* 10:11707–11735.
30. van der Werf GR, et al. (2017) Global fire emissions estimates during 1997-2016. *Earth Syst Sci Data* 9:697–720.
31. Akagi SK, et al. (2011) Emission factors for open and domestic biomass burning for use in atmospheric models. *Atmos Chem Phys* 11:4039–4072.
32. Monks SA, et al. (2015) Multi-model study of chemical and physical controls on transport of anthropogenic and biomass burning pollution to the Arctic. *Atmos Chem Phys* 15:3575–3603.
33. Etiope G (2012) Climate science: Methane uncovered. *Nat Geosci* 5:373–374.
34. Bock M, et al. (2017) Glacial/interglacial wetland, biomass burning, and geologic methane emissions constrained by dual stable isotopic CH_4 ice core records. *Proc Natl Acad Sci USA* 114:E5778–E5786.
35. Dlugokencky, EJ, et al. (2017) Atmospheric methane dry air mole fractions from the NOAA ESRL carbon cycle cooperative global air sampling network, 1983-2016. Version 2017-07-28. Available at ftp://aftp.cmdl.noaa.gov/products/trends/ch4/ch4_annmean_gl.txt. Accessed April 24, 2018.
36. Mann ME, et al. (2009) Global signatures and dynamical origins of the little ice age and medieval climate anomaly. *Science* 326:1256–1260.
37. van Marle MJE, et al. (2017) Historic global biomass burning emissions for CMIP6 (BB4CMIP) based on merging satellite observations with proxies and fire models (1750-2015). *Geosci Model Dev* 10:3329–3357.
38. Aydin M, Williams MB, Saltzman ES (2007) Feasibility of reconstructing paleoatmospheric records of selected alkanes, methyl halides, and sulfur gases from Greenland ice cores. *J Geophys Res* 112:D07312.
39. Lamarque JF, et al. (2010) Historical (1850-2000) gridded anthropogenic and biomass burning emissions of reactive gases and aerosols: Methodology and application. *Atmos Chem Phys* 10:7017–7039.
40. Sander SP, et al. (2006) Chemical kinetics and photochemical data for use in atmospheric studies, evaluation no. 15 (Jet Propulsion Lab, Pasadena, CA), JPL Publication 06-2.
41. Schwietzke S, et al. (2016) Upward revision of global fossil fuel methane emissions based on isotope database. *Nature* 538:88–91.
42. Spivakovsky CM, et al. (2000) Three-dimensional climatological distribution of tropospheric OH: Update and evaluation. *J Geophys Res* 105:8931–8980.
43. Prather MJ, Holmes CD, Hsu J (2012) Reactive greenhouse gas scenarios: Systematic exploration of uncertainties and the role of atmospheric chemistry. *Geophys Res Lett* 39:L09803.